EDGE ARTICLE

Tuning the reactivity of mononuclear nonheme manganese(IV)-oxo complexes by triflic acid†

Junying Chen,[a] Heejung Yoon,[b] Yong-Min Lee,[a] Mi Sook Seo,[a] Ritimukta Sarangi,[c] Shunichi Fukuzumi*[ab] and Wonwoo Nam*[a]

Triflic acid (HOTf)-bound nonheme Mn(IV)-oxo complexes, $[(L)Mn^{IV}(O)]^{2+}$–$(HOTf)_2$ (L = N4Py and Bn-TPEN; N4Py = N,N-bis(2-pyridylmethyl)-N-bis(2-pyridyl)methylamine and Bn-TPEN = N-benzyl-N,N',N'-tris-(2-pyridylmethyl)ethane-1,2-diamine), were synthesized by adding HOTf to the solutions of the $[(L)Mn^{IV}(O)]^{2+}$ complexes and were characterized by various spectroscopies. The one-electron reduction potentials of the Mn(IV)(O) complexes exhibited a significant positive shift upon binding of HOTf. The driving force dependences of electron transfer (ET) from electron donors to the Mn(IV)(O) and Mn(IV)(O)–(HOTf)_2 complexes were examined and evaluated in light of the Marcus theory of ET to determine the reorganization energies of ET. The smaller reorganization energies and much more positive reduction potentials of the $[(L)Mn^{IV}(O)]^{2+}$–$(HOTf)_2$ complexes resulted in greatly enhanced oxidation capacity towards one-electron reductants and para-X-substituted-thioanisoles. The reactivities of the Mn(IV)-oxo complexes were markedly enhanced by binding of HOTf, such as a 6.4×10^5-fold increase in the oxygen atom transfer (OAT) reaction (i.e., sulfoxidation). Such a remarkable acceleration in the OAT reaction results from the enhancement of ET from para-X-substituted-thioanisoles to the Mn(IV)(O) complexes as revealed by the unified ET driving force dependence of the rate constants of OAT and ET reactions of $[(L)Mn^{IV}(O)]^{2+}$–$(HOTf)_2$. In contrast, deceleration was observed in the rate of H-atom transfer (HAT) reaction of $[(L)Mn^{IV}(O)]^{2+}$–$(HOTf)_2$ complexes with 1,4-cyclohexadiene as compared with those of the $[(L)Mn^{IV}(O)]^{2+}$ complexes. Thus, the binding of two HOTf molecules to the Mn(IV)(O) moiety resulted in remarkable acceleration of the ET rate when the ET is thermodynamically feasible. When the ET reaction is highly endergonic, the rate of the HAT reaction is decelerated due to the steric effect of the counter anion of HOTf.

Introduction

High-valent metal-oxo species have been invoked as key intermediates in biological and chemical oxidation reactions.[1–5] In particular, high-valent manganese-oxo species have attracted much attention recently as an essential species in the oxygen-evolving complex (OEC) in photosystem II (PS II), which contains a redox-inactive Ca^{2+} ion in addition to redox-active Mn ions as cofactors.[6–8] In biomimetic studies, the reactivities of metal-oxo complexes have been investigated in various oxidation reactions such as oxygen atom transfer (OAT) and

hydrogen atom transfer (HAT) reactions.[1–5,9] It has been demonstrated that the reactivities of high-valent metal-oxo complexes are affected by various factors such as the structure and topology of supporting ligands, the identity of axial ligands, and the spin state of metal ions.[9,10] The reactivity of metal-oxo complexes has been further enhanced by binding of a redox-inactive metal ions to the metal-oxo moiety, indicating that metal-oxo complexes act as very powerful oxidants by binding of redox-inactive metal ions.[10–13] Binding of a redox-inactive metal ion acting as a Lewis acid to a high-valent metal-oxo complex has been confirmed by the crystal structure of a Sc^{3+} ion-bound nonheme iron(IV)-oxo complex, $[(TMC)Fe^{IV}(O)]^{2+}$ (TMC = 1,4,8,11-tetramethyl-1,4,8,11-tetraazacyclotetradecane).[14] In general, binding metal ions to oxygen and nitrogen atoms of C=O and C=N bonds of organic compounds as well as metal-oxo complexes results in enhancement of their reactivity towards electron donors, caused by a positive shift of the one-electron reduction potentials of metal ion-bound electron acceptors.[15,16] Not only metal ions but also Brønsted acids, such as perchloric acid ($HClO_4$) and trifluoromethanesulfonic acid (HOTf), accelerate electron transfer from electron donors to electron

[a]Department of Chemistry and Nano Science, Department of Bioinspired Science, Center for Biomimetic System, Ewha Womans University, Seoul 120-750, Korea. E-mail: wwnam@ewha.ac.kr

[b]Department of Material and Life Science, Graduate School of Engineering, ALCA, JST, Osaka University, Suita, Osaka 565-0871, Japan. E-mail: fukuzumi@chem.eng.osaka-u.ac.jp

[c]Stanford Synchrotron Radiation Lightsource, SLAC National Accelerator Laboratory, Menlo Park, California 94025, USA

acceptors including metal-oxo complexes when acids bind to the one-electron-reduced species of electron acceptors.[15–18] The acceleration effects of Brønsted acids on the reactivity of electron acceptors towards electron donors are expected to be maximized when electron acceptors are protonated prior to electron transfer.[19] In the catalytic cycles of metalloenzymes, Brønsted acids play a very important role in controlling the reactivity of high-valent metal-oxo intermediates *via* hydrogen bonding.[20,21] However, evidence for the direct binding of Brønsted acids to high-valent metal-oxo complexes has yet to be obtained.

We report herein the first spectroscopic evidence for binding of two HOTf molecules to mononuclear nonheme Mn(IV)-oxo complexes, $[(N4Py)Mn^{IV}(O)]^{2+}$ and $[(Bn-TPEN)Mn^{IV}(O)]^{2+}$ (N4Py = *N*,*N*-bis(2-pyridylmethyl)-*N*-bis(2-pyridyl)methylamine and Bn-TPEN = *N*-benzyl-*N*,*N'*,*N'*-tris(2-pyridylmethyl)ethane-1,2-diamine) to produce $[(L)Mn^{IV}(O)]^{2+}$–(HOTf)$_2$ (L = N4Py and Bn-TPEN) (see Fig. 1). The binding of two HOTf molecules to $[(L)Mn^{IV}(O)]^{2+}$ enhanced the reactivity of $[(L)Mn^{IV}(O)]^{2+}$ dramatically in electron transfer (ET) reaction with one-electron reductants as well as in OAT reaction with thioanisoles. In contrast, the reactivity of $[(L)Mn^{IV}(O)]^{2+}$–(HOTf)$_2$ decreased significantly in the HAT reaction with 1,4-cyclohexadiene. A large positive shift of the one-electron reduction potentials of the Mn^{IV}(O) complexes was also observed upon binding of two HOTf molecules to the Mn^{IV}(O) complexes, resulting from the much larger binding constants of HOTf to the one-electron reduced species, $([(L)Mn^{III}(O)]^+)$, as compared with those of $[(L)Mn^{IV}(O)]^{2+}$. A unified ET driving force dependence of the rate constants of ET and OAT reactions of $[(L)Mn^{IV}(O)]^{2+}$–(HOTf)$_2$, which were analyzed in light of the Marcus theory of electron transfer,[22] provides valuable insights into the change in the mechanism depending on the ET driving force.

Results and discussion

Binding of HOTf to nonheme Mn^{IV}(O) complexes

Mononuclear high-valent Mn^{IV}(O) complexes, $[(N4Py)Mn^{IV}(O)]^{2+}$ (1) and $[(Bn-TPEN)Mn^{IV}(O)]^{2+}$ (2), were generated by reacting $[(N4Py)Mn^{II}]^{2+}$ and $[(Bn-TPEN)Mn^{II}]^{2+}$ with iodosylbenzene (PhIO), respectively, as reported previously.[23–25] Addition of HOTf to an *in situ* generated solution of 1 in CF$_3$CH$_2$OH–CH$_3$CN (v/v = 1 : 1) at 273 K afforded a reddish brown solution and resulted in the disappearance of the absorption band at 940 nm due to 1, accompanied by a new absorption

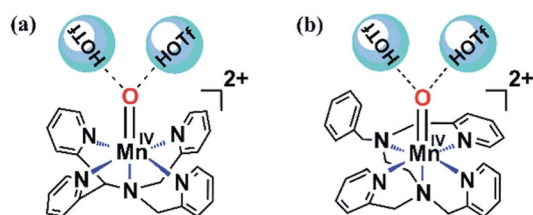band formation at 550 nm (shoulder, $\varepsilon = 540$ M^{-1} cm^{-1}) (Fig. 2). Similar spectral changes were also obtained for 2, indicating that the absorption band at 1020 nm due to 2 disappeared and concomitantly a new absorption band at 580 nm ($\varepsilon = 600$ M^{-1} cm^{-1}) was generated (see Fig. S1, ESI†).

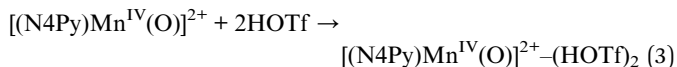The spectral titration of 1 with HOTf (Fig. 2) exhibits a sigmoidal curvature (inset of Fig. 2), which suggests that more than one HOTf are attached to 1. In such a case, the absorption change (ΔA) due to binding of n molecules of HOTf to 1 is given by eqn (1),

$$\Delta A = \Delta A_0 K[\text{HOTf}]^n/(1 + K[\text{HOTf}]^n) \quad (1)$$

where ΔA_0 is the final absorption change due to binding of n molecules of HOTf to 1 and K is the binding constant. Eqn (1) is rewritten as eqn (2),

$$\log(\Delta A/(\Delta A_0 - \Delta A)) = \log K + n(\log[\text{HOTf}]) \quad (2)$$

which predicts a linear correlation between $\log(\Delta A/(\Delta A_0 - \Delta A))$ and $\log[\text{HOTf}]$ with a slope of n. From a linear correlation of $\log(\Delta A/(\Delta A_0 - \Delta A))$ *vs.* $\log[\text{HOTf}]$, the number of HOTf molecules bound to 1 and the binding constant were determined to be 2.0(1) and $1.3(3) \times 10^5$ M^{-2}, where $\log K = 5.1(1)$, respectively (inset of Fig. 2 for the fitting of spectral titration data; Fig. S2, ESI† for linear plot using eqn (2)). Thus, 1 is bound to two HOTf molecules to afford the HOTf-bound species, $[(N4Py)Mn^{IV}(O)]^{2+}$–(HOTf)$_2$ (3) [eqn (3)], which is relatively stable at 273 K ($t_{1/2} \approx 6$ h; see Fig. S3, ESI†).

$$[(N4Py)Mn^{IV}(O)]^{2+} + 2\text{HOTf} \rightarrow$$
$$[(N4Py)Mn^{IV}(O)]^{2+}–(\text{HOTf})_2 \quad (3)$$

When 2 was bound to two HOTf molecules to form the HOTf-bound species, $[(Bn-TPEN)Mn^{IV}(O)]^{2+}$–(HOTf)$_2$ (4), the half-life-time of 4 was 1.5 h, indicating 4 is somewhat less stable than 3 (Fig. S3, ESI†). It is important to note that 3 and 4 reverted to 1 and 2, respectively, upon addition of base (*i.e.*, triethylamine) as shown in Fig. S4, ESI.†

Fig. 1 Schematic drawing of the chemical structures of $[(N4Py)Mn^{IV}(O)]^{2+}$ (a) and $[(Bn-TPEN)Mn^{IV}(O)]^{2+}$ (b) species binding two HOTf molecules.
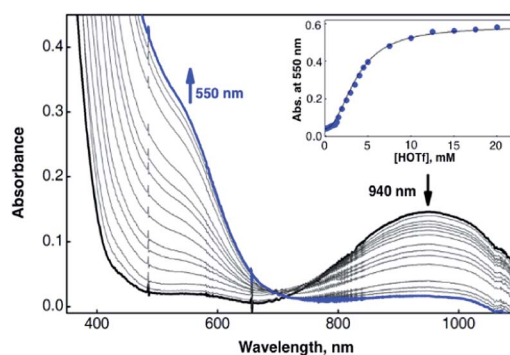

Fig. 2 UV-vis spectral changes observed in the titration of 1 (black bold line) with HOTf. HOTf (0–20 mM) was added incrementally into the solution of 1 (0.50 mM) in CF$_3$CH$_2$OH–CH$_3$CN (v/v = 1 : 1) at 273 K. Inset shows the spectral titration monitored at 550 nm (blue circles) due to the formation of 3.

The X-band EPR spectrum of **3** exhibits signals that are characteristic of $S = 3/2$ Mn^{IV} ($g_1 = 5.8$, $g_2 = 3.2$ and $g_3 = 2.01$; see Fig. S5, ESI†). The magnetic moment of **3** was also determined to be 4.3 μ_B by the modified ^1H NMR technique of Evans,[26] confirming the spin state of $S = 3/2$. The cold-spray ionization time-of-flight mass (CSI-TOF MS) spectrum of **3** exhibits ion peaks at m/z 737.0 and 759.0, which shift to 739.0 and 761.0 upon introduction of ^{18}O during the generation of **3** using $PhI^{18}O$ (Fig. S6, ESI†). This ^{18}O-labeled experiment suggests that **3** contains one oxygen atom. It should be noted that a species containing one bound HOTf was detected in CSI-TOF MS spectra, but the species with two bound HOTf molecules was not detected, probably because the binding of HOTf is fragile and easily broken under the CSI-TOF MS conditions.

Comparison of X-ray absorption near edge structure (XANES) at the Mn K-edge for $[(N4Py)Mn^{IV}(O)]^{2+}$ (**1**, red line in Fig. 3a) and $[(N4Py)Mn^{IV}(O)]^{2+}$–(HOTf)$_2$ (**3**, black line in Fig. 3a) clearly shows a decrease in pre-edge intensity and no change in the rising-edge energy position of **3** relative to **1**, which is consistent with the elongation of the Mn–O bond and unchanged Mn^{IV} oxidation state, also consistent with the EPR results (Fig. S5, ESI†). Extended X-ray absorption fine structure (EXAFS) data as shown in Fig. 3b indicate a short Mn–O bond distance of 1.74 Å (see Tables S1 and S2, ESI†). This is longer than the 1.67 Å observed in $[(N4Py)Mn^{IV}(O)]^{2+}$ (**1**), indicating that the HOTf molecules interact with the oxo moiety of **1**. This Mn–O bond distance in **3** is almost identical to that of the $[(N4Py)Mn^{IV}(O)]^{2+}$ complex binding Sc^{3+} ions.[23,24] It should be noted that protons are not dissociated from the two HOTf moieties in Mn=O···

(HOTf)$_2$, instead they are coordinated to the Mn^{IV}=O unit by hydrogen bonding interaction. It is distinct from diprotonation, which would yield the putatively unstable $[Mn^{IV}(OH_2)]^{4+}$ species. This is evidenced by the small change in Mn=O distance upon binding of two HOTf molecules (less than 0.1 Å). The Mn–O distance of 1.74 Å indicates the double bond character of Mn–O, somewhat weakened by hydrogen bonding.

Thermodynamic and kinetic evidence for binding of HOTf to $[(N4Py)Mn^{IV}(O)]^{2+}$ (**1**)

Binding of two HOTf molecules to **1** was supported by the kinetic studies on the oxidation of *para*-CN-thioanisole by **3**, which was prepared by adding different amounts of HOTf (0–50 mM) into a solution of **1** (0.50 mM). The observed second-order rate constants (k_2) were determined by monitoring a decrease in absorption bands at 550 nm due to **3** or 940 nm due to **1**. The dependence of the second-order rate constant for the oxidation of *para*-CN-thioanisole on the concentration of HOTf shows a sigmoidal curvature as shown in Fig. 4. Such a sigmoidal curvature can be well explained by eqn (4),

$$k_2 = k_{ox}K[HOTf]^2/(1 + K[HOTf]^2) \qquad (4)$$

where k_{ox} is the rate constant of OAT from **3** to *para*-CN-thioanisole. Eqn (4) is rewritten as eqn (5), which predicts a linear relation between k_2^{-1} and $[HOTf]^{-2}$.

$$k_2^{-1} = (k_{ox}K)^{-1}[HOTf]^{-2} + k_{ox}^{-1} \qquad (5)$$

A linear plot of k_2^{-1} *vs.* $[HOTf]^{-2}$ (Fig. S7, ESI†) afforded the k_{ox} and K values of 2.5 M^{-1} s^{-1} and 1.6(4) $\times$ 10^5 M^{-2} [log $K = 5.2(1)$], respectively, determined from the slope and intercept. The K value determined from the inset of Fig. 4 or S7, ESI† is quite consistent with the value determined from the spectral titration under the same experimental conditions (Fig. S2, ESI†). Furthermore, the fitting line in Fig. 4 obtained by using the k_{ox} and K values determined is well matched with
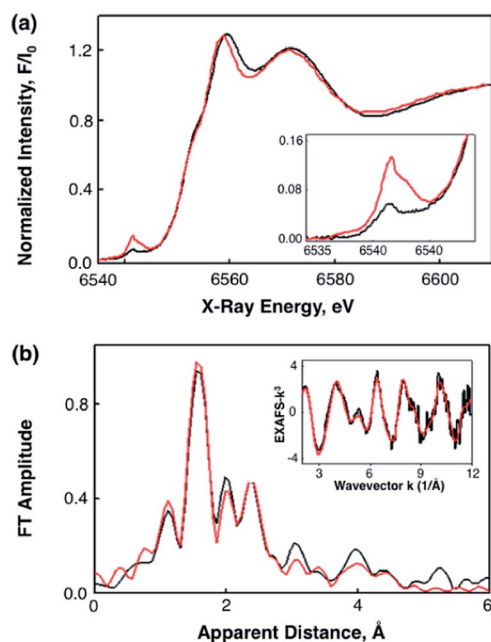

Fig. 3 (a) Normalized Mn K-edge XANES of **1** (red line) and **3** with 30 mM of HOTf (black line). Inset shows magnified pre-edge features. (b) Non-phase-shift corrected Fourier transforms (black line) and the corresponding Mn K-edge EXAFS data (inset; black line) for **3**. Fits (red lines) were performed in the range of $k = 2$–12 Å^{-1}.
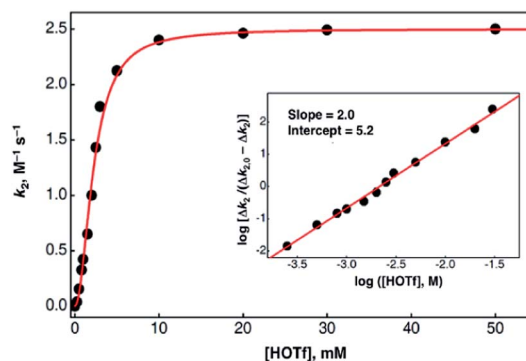

Fig. 4 Dependence of the second-order rate constant, k_2, for the oxidation of *para*-CN-thioanisole by **3** (0.50 mM) on [HOTf] (0–50 mM) in CF_3CH_2OH–CH_3CN (v/v = 1 : 1) at 273 K. Inset shows a plot of log[$\Delta k_2/(\Delta k_{2,0} - \Delta k_2)$] *vs.* log[HOTf], where $\Delta k_{2,0}$ is the full change of second-order rate constant.
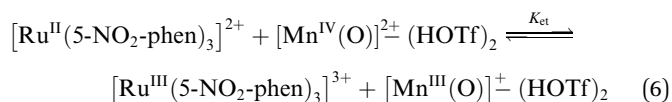
experimental data points, clearly indicating that two molecules of HOTf are involved in these reactions.

Enhancement of the oxidation capacity of the nonheme $Mn^{IV}(O)$ complexes by binding of two HOTf molecules

Electron transfer from coordinatively saturated metal complexes to $[Mn^{IV}(O)]^{2+}$–$(HOTf)_2$ complexes, **3** and **4**, were investigated, and these **3** and **4** species were found to perform electron transfer (ET) reaction with the one-electron reductant, $[Ru^{II}(5\text{-}NO_2\text{-}phen)_3](PF_6)_2$ (5-NO₂-phen: 5-nitro-1,10-phenanthroline), which has a one-electron oxidation potential as high as 1.50 V vs. SCE, whereas no ET was observed for **1** ($E_{red} = 0.80$ V vs. SCE) and **2** ($E_{red} = 0.78$ V vs. SCE).[24] The redox titration for formation of $[Ru^{III}(5\text{-}NO_2\text{-}phen)_3]^{3+}$, as shown in Fig. 5, indicates only one-electron reduction of **3** occurred without further reduction by $[Ru^{II}(5\text{-}NO_2\text{-}phen)_3]^{2+}$. Upon addition of $[Ru^{II}(5\text{-}NO_2\text{-}phen)_3]^{2+}$ into a solution of **3**, the absorption band at 450 nm due to $[Ru^{II}(5\text{-}NO_2\text{-}phen)_3]^{2+}$ disappeared (data not shown) and concomitantly the absorption band at 650 nm due to $[Ru^{III}(5\text{-}NO_2\text{-}phen)_3]^{3+}$ appeared with an isosbestic point at 550 nm (Fig. 5a). By analyzing the resulting solution by EPR, we found that a Mn^{III} species was formed as a major product in the ET reaction by **3** (Fig. S8, ESI†). It should be noted that the second ET could be observed to form the Mn^{II} product when a large excess of $[Ru^{II}(5\text{-}NO_2\text{-}phen)_3]^{2+}$ was used; however, the rate of the second ET is much slower than that of the first ET at 273 K. The titration curve of the ET reaction, as shown in Fig. 5b, revealed that ET from $[Ru^{II}(5\text{-}NO_2\text{-}phen)_3]^{2+}$ to **3** is in

equilibrium with back electron transfer from the $[Mn^{III}(O)]^+$–$(HOTf)_2$ species to $[Ru^{III}(5\text{-}NO_2\text{-}phen)_3]^{3+}$ (eqn (6), where K_{et} is the electron-transfer equilibrium constant).

$$[Ru^{II}(5\text{-}NO_2\text{-}phen)_3]^{2+} + [Mn^{IV}(O)]^{2+}_{-}(HOTf)_2 \xrightleftharpoons{K_{et}}$$
$$[Ru^{III}(5\text{-}NO_2\text{-}phen)_3]^{3+} + [Mn^{III}(O)]^+_{-}(HOTf)_2 \quad (6)$$

By analyzing a linear plot as shown in Fig. S9c, ESI,† which was obtained from the redox titration curve in Fig. 5b, the K_{et} value was determined to be 330. The one-electron reduction potential (E_{red}) of **3** in CF_3CH_2OH–CH_3CN (v/v = 1 : 1) at 273 K was then determined from the K_{et} value and the E_{ox} value of $[Ru^{II}(5\text{-}NO_2\text{-}phen)_3]^{2+}$ ($E_{ox} = 1.50$ V vs. SCE) using the Nernst equation [eqn (7)],[27,28] where R is the gas constant, T is the absolute temperature, and F is the Faraday constant, to be 1.65 V vs. SCE in the presence of HOTf (30 mM).

$$E_{red} = E_{ox} + (RT/F)\ln(K_{et}) \quad (7)$$

Similarly, the E_{red} value of **4** was determined from the K_{et} value of 1.2, which was obtained by the redox titration with $[Ru^{II}(5\text{-}NO_2\text{-}phen)_3]^{2+}$ (see Fig. S10, ESI†), to be 1.50 V vs. SCE in the presence of HOTf (30 mM). Further, the E_{red} values of **3** at different concentrations of HOTf were also determined from the K_{et} values obtained by the redox titrations with $[Ru^{II}(5\text{-}Cl\text{-}phen)_3]^{2+}$ (5-Cl-phen = 5-chloro-1,10-phenanthroline; $E_{ox} = 1.41$ V vs. SCE) and $[Ru^{II}(5\text{-}NO_2\text{-}phen)_3]^{2+}$ (see Fig. S9 and S11, ESI†). Fig. 6 shows the dependence of E_{red} of **3** on the concentration of HOTf (Table S3, ESI†). The E_{red} value increases with increasing the concentration of HOTf to reach the constant value of 1.65 V vs. SCE at more than 30 mM of HOTf at 273 K. The saturated E_{red} value of 1.65 V vs. SCE in the presence of a large excess of HOTf corresponds to that of the $[Mn^{IV}(O)]^{2+}$–$(HOTf)_2$ complex of **3**. There is a large difference ($\Delta E_{red} = 0.85$ V in the case of N4Py) in the E_{red} values between $[Mn^{IV}(O)]^{2+}$ and $[Mn^{IV}(O)]^{2+}$–$(HOTf)_2$, which indicates that the binding of HOTf to $[Mn^{III}(O)]^+$ (the species derived from one-electron reduction of $[Mn^{IV}(O)]^{2+}$) is much stronger than that to $[Mn^{IV}(O)]^{2+}$, as expected from the increased basicity of the oxo moiety in $[Mn^{III}(O)]^+$. Thus, the HOTf-bound $Mn^{IV}(O)$ complex
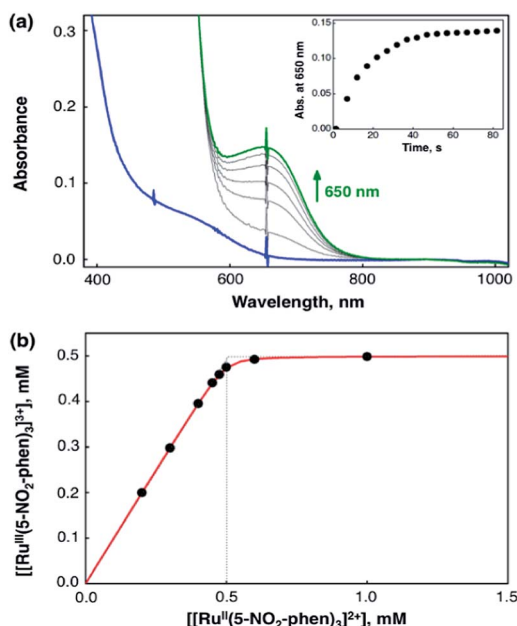

Fig. 5 (a) UV-vis spectral changes for **3** (0.10 mM) upon addition of $[Ru^{II}(5\text{-}NO_2\text{-}phen)_3](PF_6)_2$ (1.0 mM) in the presence of HOTf (30 mM) in CF_3CH_2OH–CH_3CN (v/v = 1 : 1) at 273 K. The inset shows the time trace monitored at 650 nm due to the formation of $[Ru^{III}(5\text{-}NO_2\text{-}phen)_3]^{3+}$. (b) Plot of concentration of $[Ru^{III}(5\text{-}NO_2\text{-}phen)_3]^{3+}$ produced in electron transfer from $[Ru^{II}(5\text{-}NO_2\text{-}phen)_3]^{2+}$ (1.50 V vs. SCE) to **3** (0.50 mM) in the presence of HOTf (30 mM) at 273 K.
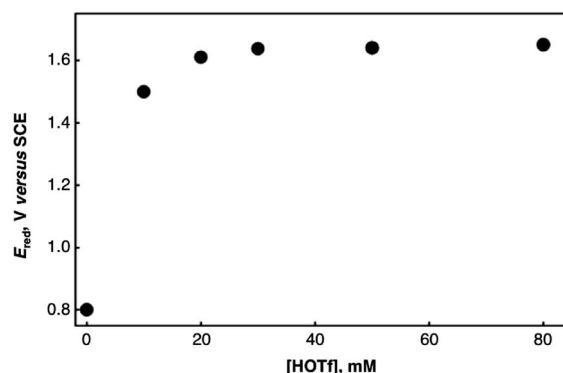

Fig. 6 Dependence of E_{red} of $[(N4Py)Mn^{IV}(O)]^{2+}$ on the concentration of HOTf (0–80 mM) in CF_3CH_2OH–CH_3CN (v/v = 1 : 1) at 273 K.

acts as the strongest oxidant among the nonheme Mn-oxo complexes bearing the same ligand system.

As compared with the E_{red} values of $[(N4Py)Mn^{IV}(O)]^{2+}$ (0.80 V vs. SCE) and $[(N4Py)Mn^{IV}(O)]^{2+}$–$(Sc^{3+})_2$ (1.42 V vs. SCE),[24] a remarkable positive shift of E_{red} of **3** (1.65 V vs. SCE) was observed under the same conditions in CF_3CH_2OH–CH_3CN (v/v = 1 : 1) at 273 K, resulting in significant enhancement of the ET reactivity. Rates of ET from various one-electron donors, coordinatively saturated iron(II) and ruthenium(II) complexes, to **3** and **4** were investigated and the rate constants were determined by monitoring the absorbance changes due to the decay of iron(II) or the formation of corresponding ruthenium(III) species. Rates of ET obeyed pseudo-first-order or second-order kinetics, and the pseudo-first-order rate constant (k_{obs}) increased linearly with increasing concentrations of electron donors. The second-order rate constants (k_{et}) of ET thus determined are listed in Table 1 together with the one-electron oxidation potentials (E_{ox}) of one-electron reductants in CF_3-CH_2OH–CH_3CN (v/v = 1 : 1) and the driving force of ET ($-\Delta G_{et}$) (see also Fig. S12 and S13, ESI,† for **3** and **4**, respectively).

Outer-sphere electron transfer of $[Mn^{IV}(O)]^{2+}$–$(HOTf)_2$

The driving force dependence of the rate constants of electron transfer from one-electron reductants to **3** (Fig. 7 and Table 1) is well fitted in the light of the Marcus theory of adiabatic outer-sphere electron transfer [eqn (8)],
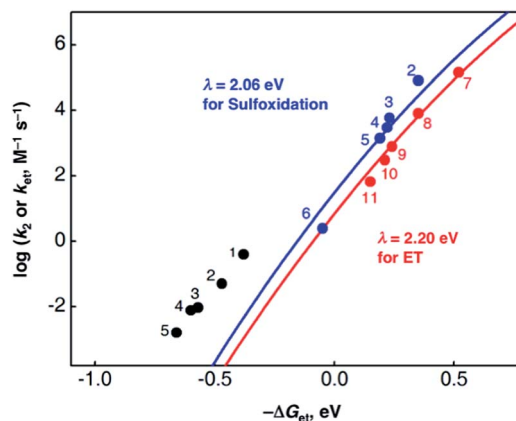

Fig. 7 Plots of log k_2 for sulfoxidation of *para*-X-substituted thioanisoles [X = (1) MeO, (2) Me, (3) H, (4) F, (5) Br and (6) CN] by $[(N4Py)Mn^{IV}(O)]^{2+}$ vs. the driving force of electron transfer $[-\Delta G_{et} = e(E_{red} - E_{ox})]$ from thioanisoles to $[(N4Py)Mn^{IV}(O)]^{2+}$ in the absence of HOTf (black circles)[21,22] and the presence of 30 mM of HOTf (blue circles) in CF_3CH_2OH–CH_3CN (v/v = 1 : 1) at 273 K. The red circles show the driving force dependence of the rate constants (log k_{et}) of ET from one-electron reductants [(7) $[Ru^{II}(Me_2-bpy)_3](PF_6)_2$, (8) $[Ru^{II}(bpy)_3](PF_6)_2$, (9) $[Ru^{II}(5-Cl-phen)_3](PF_6)_2$, (10) $[Ru^{II}(5-Br-bpy)_3](PF_6)_2$ and (11) $[Ru^{II}(5-NO_2-phen)_3](PF_6)_2)]$ to $[(N4Py)Mn^{IV}(O)]^{2+}$ in the presence of 30 mM of HOTf in CF_3CH_2OH–CH_3CN (v/v = 1 : 1) at 273 K.

Table 1 One-electron oxidation potentials (E_{ox}) of one-electron reductants and *para*-X-substituted thioanisoles and second-order rate constants of ET and sulfoxidation reactions by $[(N4Py)Mn^{IV}(O)]^{2+}$–$(HOTf)_2$ (**3**) and $[(Bn-TPEN)Mn^{IV}(O)]^{2+}$–$(HOTf)_2$ (**4**) with driving force of ET ($-\Delta G_{et}$) in the presence of HOTf (30 mM) in CF_3CH_2OH–CH_3CN (v/v = 1 : 1) at 273 K

Electron donor	$E_{ox}{}^a$ (V vs. SCE)	$[(N4Py)Mn^{IV}(O)]^{2+}$–$(HOTf)_2$		$[(Bn-TPEN)Mn^{IV}(O)]^{2+}$–$(HOTf)_2$	
		k_{et}, M^{-1} s^{-1}	$-\Delta G_{et}$, eV	k_{et}, M^{-1} s^{-1}	$-\Delta G_{et}$, eV
$[Fe^{II}(Me_2-bpy)_3]^{2+}$	0.92	Too fast	0.73	4.3×10^5	0.58
$[Fe^{II}(bpy)_3]^{2+}$	1.09	Too fast	0.56	4.5×10^4	0.41
$[Fe^{II}(phen)_3]^{2+}$	1.11	Too fast	0.54	4.7×10^4	0.39
$[Ru^{II}(Me_2-bpy)_3]^{2+}$	1.13	1.4×10^5	0.52	3.6×10^3	0.37
$[Ru^{II}(bpy)_3]^{2+}$	1.30	8.0×10^3	0.35	c	0.20
$[Ru^{II}(5-Cl-phen)_3]^{2+}$	1.41	7.8×10^2	0.24	9.2×10^2	0.09
$[Ru^{II}(5-Br-bpy)_3]^{2+}$	1.44	3.0×10^2	0.21	2.6×10^2	0.06
$[Ru^{II}(5-NO_2-phen)_3]^{2+}$	1.50	6.5×10	0.15	Too slow	0

X in *para*-X-thioanisole	$E_{ox}{}^b$ (V vs. SCE)	$[(N4Py)Mn^{IV}(O)]^{2+}$–$(HOTf)_2$		$[(Bn-TPEN)Mn^{IV}(O)]^{2+}$–$(HOTf)_2$	
		k_2, M^{-1} s^{-1}	$-\Delta G_{et}$, eV	k_2, M^{-1} s^{-1}	$-\Delta G_{et}$, eV
Me	1.30	8.1×10^4	0.35	c	0.20
H	1.42	5.9×10^3	0.23	5.5×10^3	0.08
F	1.43	3.0×10^3	0.22	3.8×10^3	0.07
Br	1.47	1.4×10^3	0.18	3.4×10^3	0.03
CN	1.70	2.5	-0.05	1.2×10	-0.20
NO$_2$	1.74	c	-0.09	3.4	-0.24

^{a} The one-electron oxidation potentials of coordinatively saturated metal complexes were determined by cyclic voltammetry in CF_3CH_2OH–CH_3CN (v/v = 1 : 1) containing 0.10 M n-Bu$_4$NPF$_6$ as a supporting electrolyte at 298 K. The one-electron oxidation potentials of coordinatively saturated metal complexes in the presence of HOTf (30 mM) were identical to those in the absence of HOTf. ^{b} The one-electron oxidation potentials of *para*-X-thioanisoles were determined by second harmonic A.C. voltammetry (SHACV) in CF_3CH_2OH–CH_3CN (v/v = 1 : 1) containing 0.10 M n-Bu$_4$NPF$_6$ as a supporting electrolyte at 298 K. ^{c} Not measured.

$$k_{et} = Z \exp[-(\lambda/4)(1 + \Delta G_{et}/\lambda)^2/k_B T] \quad (8)$$

where Z is the collision frequency, taken as 1×10^{11} M^{-1} s^{-1}, λ is the reorganization energy of electron transfer, k_B is the Boltzmann constant, and T is the absolute temperature. From the fitting of the ET rate constants (red circles in Fig. 7), the λ value of ET from one-electron reductants to **3** was determined to be 2.20 ± 0.02 eV. Similarly, the λ value for the ET reaction of **4** with one-electron reductants was determined to be 2.15 ± 0.03 eV (Table 1; see also Fig. S13 and S14, ESI†). Both λ values of the ET reduction of $[(L)Mn^{IV}(O)]^{2+}$–$(HOTf)_2$ (L = N4Py and Bn-TPEN) are smaller than those of $[(L)Mn^{IV}(O)]^{2+}$ in the absence of HOTf,[24,25] since the elongation of the Mn–O bond distance by binding of two HOTf molecules occurs prior to the ET, resulting in a smaller change in the Mn–O bond distance after ET reduction. However, the λ values for $[Mn^{IV}(O)]^{2+}$–$(HOTf)_2$ are quite similar to those for $[Mn^{IV}(O)]^{2+}$–$(Sc^{3+})_2$.[24] This result is quite reasonable because, according to the XANES/EXAFS analyses, the elongation of the Mn–O bond due to binding of HOTf is almost identical to the case of the Mn–O species binding Sc^{3+} ions (*vide supra*).[23]

Contrasting effects of binding of HOTf on the reactivity of nonheme Mn^{IV}(O) complexes in OAT and HAT reactions

The reactivity of the HOTf-bound Mn^{IV}(O) complexes, **3** and **4**, was investigated in OAT and HAT reactions. The OAT reaction (*e.g.*, the oxidation of thioanisoles) was markedly influenced by binding of two HOTf molecules to the Mn-oxo moiety (Table 1; Fig. S15 and S16, ESI† for **3** and **4**, respectively). Upon addition of thioanisole to a solution of **3** (Fig. 8a), the Mn^{IV}(O) complex reverted to the starting Mn^{II} complex, which was confirmed by EPR (Fig. S17, ESI†). Product analysis of the reaction solutions revealed the formation of methyl phenyl sulfoxide in a quantitative yield. These results indicate that the oxidation of thioanisole by the HOTf-bound Mn^{IV}(O) complexes, Mn^{IV}(O)–(HOTf)$_2$, occurs *via* a two-electron oxidation process as reported previously for Mn^{IV}(O) and Mn^{IV}(O)–(Sc^{3+})$_2$.[23,24] The second-order rate constant (5.9×10^3 M^{-1} s^{-1}) determined in the reaction of thioanisole with **3** at 273 K is 6.4×10^5-fold and 3.0×10^2-fold greater than those of **1** (9.2×10^{-3} M^{-1} s^{-1}) and $[(N4Py)Mn^{IV}(O)]^{2+}$–$(Sc^{3+})_2$ (2.0×10 M^{-1} s^{-1}),[23] respectively, demonstrating that the reactivity of the Mn(IV)-oxo complex in the OAT reaction is markedly enhanced by binding of two HOTf molecules. Much accelerated reactivity of the HOTf-bound Mn^{IV}(O) species was also observed in the reactions of other *para*-X-substituted thioanisoles (Table 1; Fig. S15, ESI†). In addition, a good linear correlation was obtained by plotting the log k_2 values against one-electron oxidation potentials of thioanisoles (Fig. 8b). The slope of $-11.4(5)$ in Fig. 8b is in between those reported for outer-sphere electron transfer reductions of $[(TMC)Fe^{III}$–$OOH]^{2+}$ [slope = $-9.7(6)$] and $[(TMC)Fe^{III}$–$OOC(CH_3)_3]^{2+}$ [slope = $-12(1)$],[29] suggesting that the rate dependence on the oxidation potential of the reductant follows the Marcus theory of electron transfer. The remarkable enhancement of the reactivity was also observed in the oxidation of thioanisoles by **4**. The slope in the plot of the log k_2
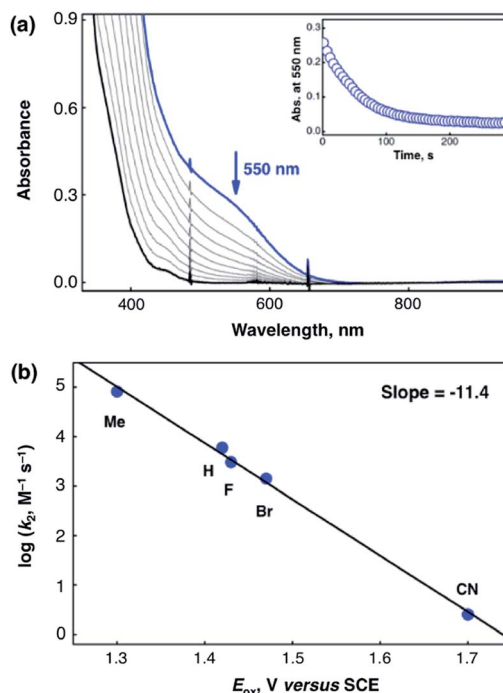

Fig. 8 (a) UV-vis spectral changes of **3** (0.50 mM) upon addition of *p*-CN-thioanisole (5.0 mM) in the presence of HOTf (30 mM) in CF$_3$-CH$_2$OH–CH$_3$CN (v/v = 1 : 1) at 273 K. Inset shows the time trace monitored at 550 nm. (b) Plot of the log k_2 against one-electron oxidation potentials of *para*-X-thioanisoles (X =Me, H, F, Br, and CN) for the oxidation of thioanisole derivatives by **3** in the presence of HOTf (30 mM) in CF$_3$CH$_2$OH–CH$_3$CN (v/v = 1 : 1) at 273 K.

values against one-electron oxidation potentials of thioanisoles (Fig. S18, ESI†) for **4** was $-10.0(6)$, which is similar to that of **3**, indicating that an ET process is involved in the rate determining step. In the OAT reaction by **3**, the rate was dependent on reaction temperature (Fig. S19, ESI†). The activation parameters of $\Delta H^{\ddagger} = 15.1$ kcal mol^{-1} and $\Delta S^{\ddagger} = -1.2$ cal mol^{-1} K^{-1} were determined from the slope and intercept in a linear Eyring plot obtained between 253 K and 293 K (Fig. S20, ESI†). The observed activation entropy close to zero is also indicative of those of outer-sphere electron-transfer reactions,[22,27] suggesting that the OAT reaction of **3** occurs *via* ET from thioanisoles to **3**.

We have shown previously the change of mechanism from a direct oxygen atom transfer (DOT) pathway by $[(N4Py)Mn^{IV}(O)]^{2+}$ to an electron transfer (ET) pathway by $[(N4Py)Mn^{IV}(O)]^{2+}$ binding two Sc^{3+} ions in the sulfoxidation of thioanisoles.[24] As shown in Fig. 7, the electron-transfer driving force dependence of log k_2 for the oxidation of thioanisoles by **3** (blue circles) exhibits virtually the same relationship with the driving force dependence of log k_{et} of electron-transfer reactions of **3** (red circles), whereas a huge deviation from the ET line for those of **1** (black circles) was shown. This result together with the slope in the plot of the log k_2 values against one-electron oxidation potentials of thioanisoles and the activation parameters (*vide supra*) strongly indicates that the oxidation of thioanisoles by Mn^{IV}(O)–(HOTf)$_2$ intermediates proceeds *via* an outer-sphere electron-transfer pathway.[25]

The reactivities of the HOTf-bound Mn-oxo species, **3** and **4**, were also investigated kinetically in HAT, such as the C–H bond activation of 1,4-cyclohexadiene (CHD). Outer-sphere electron transfer from CHD to **3** is highly endergonic and thereby unlikely to occur judging from the more positive one-electron oxidation potential of CHD ($E_{ox} = 1.89$ V $vs.$ SCE)[30] than the one-electron reduction potential of **3** ($E_{red} = 1.65$ V $vs.$ SCE). As shown in Fig. 9a, addition of CHD to a solution of **3** in CF$_3$-CH$_2$OH–CH$_3$CN (v/v = 1 : 1) at 298 K afforded the decay of absorption band at 550 nm due to **3**. Analysis of the resulting solution with EPR, GC and GC-MS showed that the major product was a Mn^{III} species, which is EPR silent (Fig. S17, ESI† for EPR),[23] and that benzene was obtained as the sole organic product with a yield of 48% based on the concentration of **3**, similar to that observed in the oxidation of CHD by nonheme Mn^{IV}(O), Mn^{IV}(O)–(Sc^{3+})$_2$ and other nonheme metal-oxo species.[23,31] The second-order rate constant (9.2×10^{-1} M^{-1} s^{-1}) determined in the oxidation of CHD by **3** was smaller, by a factor of ~4, than that for **1** (3.5 M^{-1} s^{-1}) at 298 K (Fig. 9b), indicating that the reactivity of the Mn^{IV}(O) complex is diminished by binding of two HOTf molecules to the Mn^{IV}(O) moiety. As reported previously, the reactivity of the Mn^{IV}(O) complex in the oxidation of CHD was diminished by a factor of ~180 upon binding of two Sc^{3+} ions and the reason for the significant deceleration of the rate was proposed to be owing to the steric effect of the Sc^{3+} ions.[23] The smaller deceleration (~4-fold) due to HOTf binding, as compared to the Sc(OTf)$_3$ binding, may be

explained by the smaller molecular size of HOTf than that of Sc(OTf)$_3$. The Mn^{IV}(O) moiety in $[Mn^{IV}(O)]^{2+}$–(HOTf)$_2$ can provide suitable interaction with the substrate, but the interaction was slightly hindered by binding of HOTf. However, the interaction between substrate and intermediate was more hindered by binding of Sc^{3+} ions, which has a relatively larger size, to the Mn^{IV}(O) moiety, leading to the more diminished reactivity in HAT reactions. Similarly, in the reaction of **4** with CHD, a deceleration of ~9-fold was detected by comparison of the reactivity of **2** (Fig. S21, ESI†).

The contrasting effects by binding of two HOTf molecules observed in OAT and HAT reactions were brought to light for the first time experimentally in the study of the effect of Brønsted acid. This contrasting effect in OAT and HAT reactions might give rise to the different reaction mechanisms; OAT reactions proceed via an outer-sphere electron-transfer pathway, which should not be influenced by steric hindrance, whereas HAT reactions should required the direct interaction between Mn^{IV}(O) moiety and substrates, which should be sensitive to the steric hindrance. In agreement with the results reported for the promotion effect of Lewis acid in the reaction of $[(N4Py)Fe^{IV}(O)]^{2+}$, our results also have shown that Brønsted acid has the ability to promote the ET reaction intensely efficiently, but relatively, the possibility of steric hindrance caused by binding of two HOTf molecules to the metal-oxo group should also be taken into consideration when a Brønsted acid is involved in a reaction system.

Conclusion

Mononuclear nonheme Mn^{IV}(O) complexes binding two HOTf molecules were generated for the first time and characterized by various spectroscopic techniques. Their reactivities in electron transfer (ET), oxygen atom transfer (OAT) and hydrogen atom transfer (HAT) reactions were investigated. Binding of two HOTf molecules to the Mn-oxo moiety leads to a more positive shift of the one-electron reduction potential and a contrasting effect on the reactivities in OAT and HAT reactions. The reactivity of the nonheme Mn^{IV}(O) complexes was markedly enhanced by binding of two HOTf molecules: 6.4×10^5-fold increase in OAT reaction ($i.e.$, oxygenation of thioanisole), whereas deceleration was observed in the rate of HAT reaction of Mn^{IV}(O)–(HOTf)$_2$ complexes with CHD relative to that of the corresponding Mn^{IV}(O) complexes. However, HAT was faster compared to that of the Sc^{3+} ion-bound complex, which may be explained by the relatively smaller molecular size of HOTf compared with that of Sc(OTf)$_3$, when the interaction between Mn^{IV}(O) and substrate required for HAT reactions would be less hindered. Thus, the binding of two HOTf molecules to the Mn^{IV}(O) moiety resulted in remarkable acceleration of the ET rate, when thermodynamically feasible. When the ET reaction is highly endergonic as with CHD, the rate of HAT is decelerated due to steric effects of the counter anion of HOTf.
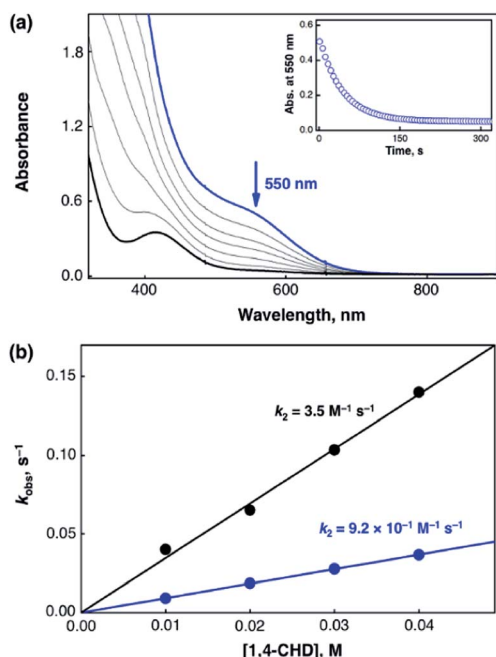

Fig. 9 (a) UV-vis spectral changes of **3** (1.0 mM) upon addition of 1,4-cyclohexadiene (CHD, 10 mM) in the presence of HOTf (30 mM) in CF$_3$CH$_2$OH–CH$_3$CN (v/v = 1 : 1) at 298 K. Inset shows the time trace monitored at 550 nm. (b) Plots of k_{obs} against the concentration of CHD to determine a second-order rate constant in the oxidation of CHD by **1** (black circles) and **3** with 30 mM of HOTf (blue circles) in CF$_3$CH$_2$OH–CH$_3$CN (v/v = 1 : 1) at 298 K.

Acknowledgements

Notes and references

1 (a) B. Meunier, S. P. de Visser and S. Shaik, *Chem. Rev.*, 2004, **104**, 3947; (b) M. M. Abu-Omar, A. Loaiza and N. Hontzeas, *Chem. Rev.*, 2005, **105**, 2227; (c) I. G. Denisov, T. M. Makris, S. G. Sligar and I. Schlichting, *Chem. Rev.*, 2005, **105**, 2253; (d) J. T. Groves, *J. Inorg. Biochem.*, 2006, **100**, 434; (e) P. R. Ortiz de Montellano, *Chem. Rev.*, 2010, **110**, 932.

2 (a) S. Shaik, S. Cohen, Y. Wang, H. Chen, D. Kumar and W. Thiel, *Chem. Rev.*, 2010, **110**, 949; (b) D. Usharani, D. Janardanan, C. Li and S. Shaik, *Acc. Chem. Res.*, 2013, **46**, 471.

3 (a) C. Krebs, D. G. Fujimori, C. T. Walsh and J. M. Bollinger Jr, *Acc. Chem. Res.*, 2007, **40**, 484; (b) L. Que Jr, *Acc. Chem. Res.*, 2007, **40**, 493; (c) W. Nam, *Acc. Chem. Res.*, 2007, **40**, 522; (d) A. S. Borovik, *Acc. Chem. Res.*, 2005, **38**, 54; (e) A. S. Borovik, *Chem. Soc. Rev.*, 2011, **40**, 1870; (f) J. Hohenberger, K. Ray and K. Meyer, *Nat. Commun.*, 2012, **3**, 720.

4 (a) P. Comba, M. Kerscher and W. Schiek, *Prog. Inorg. Chem.*, 2007, **55**, 613; (b) A. Bakac, *Coord. Chem. Rev.*, 2006, **250**, 2046; (c) J. H. Espenson, *Coord. Chem. Rev.*, 2005, **249**, 329; (d) H. Fujii, *Coord. Chem. Rev.*, 2002, **226**, 51.

5 (a) E. I. Solomon, T. C. Brunold, M. I. Davis, J. N. Kemsley, S.-K. Lee, N. Lehnert, F. Neese, A. J. Skulan, Y.-S. Yang and J. Zhou, *Chem. Rev.*, 2000, **100**, 235; (b) M. Costas, M. P. Mehn, M. P. Jensen and L. Que Jr, *Chem. Rev.*, 2004, **104**, 939; (c) E. Y. Tshuva and S. J. Lippard, *Chem. Rev.*, 2004, **104**, 987; (d) A. Decker and E. I. Solomon, *Curr. Opin. Chem. Biol.*, 2005, **9**, 152; (e) E. I. Solomon, S. D. Wong, L. V. Liu, A. Decker and M. S. Chow, *Curr. Opin. Chem. Biol.*, 2009, **13**, 99.

6 (a) M. M. Najafpour, A. N. Moghaddam, S. I. Allakhverdiev and Govindjee, *Biochim. Biophys. Acta, Bioenerg.*, 2012, **1817**, 1110; (b) B. Loll, J. Kern, W. Saenger, A. Zouni and J. Biesiadka, *Nature*, 2005, **438**, 1040.

7 (a) G. Aromi and E. K. Brechin, *Struct. Bonding*, 2006, **122**, 1; (b) R. Bagai and G. Christou, *Chem. Soc. Rev.*, 2009, **38**, 1011; (c) C. S. Mullins and V. L. Pecoraro, *Coord. Chem. Rev.*, 2008, **252**, 416; (d) S. Iwata and J. Barber, *Curr. Opin. Struct. Biol.*, 2004, **14**, 447; (e) J. Barber, *Philos. Trans. R. Soc. London, Ser. B*, 2008, **363**, 2665.

8 (a) M. Suga, F. Akita, K. Hirata, G. Ueno, H. Murakami, Y. Nakajima, T. Shimizu, K. Yamashita, M. Yamamoto, H. Ago and J.-R. Shen, *Nature*, 2015, **517**, 99; (b) Y. Umena, K. Kawakami, J.-R. Shen and N. Kamiya, *Nature*, 2011, **473**, 55; (c) K. Kawakami, Y. Umena, N. Kamiya and J.-R. Shen, *J. Photochem. Photobiol., B*, 2011, **104**, 9.

9 W. Nam, Y.-M. Lee and S. Fukuzumi, *Acc. Chem. Res.*, 2014, **47**, 1146.

10 (a) J. Kaizer, E. J. Klinker, N. Y. Oh, J.-U. Rohde, W. J. Song, A. Stubna, J. Kim, E. Münck, W. Nam and L. Que Jr, *J. Am. Chem. Soc.*, 2004, **126**, 472; (b) M. S. Seo, N. H. Kim, K.-B. Cho, J. E. So, S. K. Park, M. Clémancey, R. Garcia-Serres, J.-M. Latour, S. Shaik and W. Nam, *Chem. Sci.*, 2011, **2**, 1039; (c) S. Hong, Y.-M. Lee, K.-B. Cho, K. Sundaravel, J. Cho, M. J. Kim, W. Shin and W. Nam, *J. Am. Chem. Soc.*, 2011, **133**, 11876.

11 (a) Y. Morimoto, H. Kotani, J. Park, Y.-M. Lee, W. Nam and S. Fukuzumi, *J. Am. Chem. Soc.*, 2011, **133**, 403; (b) J. Park, Y. Morimoto, Y.-M. Lee, W. Nam and S. Fukuzumi, *J. Am. Chem. Soc.*, 2011, **133**, 5236; (c) J. Park, Y. Morimoto, Y.-M. Lee, Y. You, W. Nam and S. Fukuzumi, *Inorg. Chem.*, 2011, **50**, 11612; (d) Y. Morimoto, J. Park, T. Suenobu, Y.-M. Lee, W. Nam and S. Fukuzumi, *Inorg. Chem.*, 2012, **51**, 10025.

12 P. Leeladee, R. A. Baglia, K. A. Prokop, R. Latifi, S. P. de Visser and D. P. Goldberg, *J. Am. Chem. Soc.*, 2012, **134**, 10397.

13 (a) E. Y. Tsui, R. Tran, J. Yano and T. Agapie, *Nat. Chem.*, 2013, **5**, 293; (b) J. S. Kanady, J. L. Mendoza-Cortes, E. Y. Tsui, R. J. Nielsen, W. A. Goddard III and T. Agapie, *J. Am. Chem. Soc.*, 2013, **135**, 1073; (c) J. S. Kanady, E. Y. Tsui, M. W. Day and T. Agapie, *Science*, 2011, **333**, 733.

14 S. Fukuzumi, Y. Morimoto, H. Kotani, P. Naumov, Y.-M. Lee and W. Nam, *Nat. Chem.*, 2010, **2**, 756.

15 (a) S. Fukuzumi, *Prog. Inorg. Chem.*, 2009, **56**, 49; (b) S. Fukuzumi, *Bull. Chem. Soc. Jpn.*, 1997, **70**, 1; (c) S. Fukuzumi and K. Ohkubo, *Coord. Chem. Rev.*, 2010, **254**, 372; (d) S. Fukuzumi, *Chem. Lett.*, 2008, **37**, 808; (e) S. Fukuzumi, H. Ohtsu, K. Ohkubo, S. Itoh and H. Imahori, *Coord. Chem. Rev.*, 2002, **226**, 71; (f) S. Fukuzumi and S. Itoh, *Antioxid. Redox Signaling*, 2001, **3**, 807.

16 (a) S. Fukuzumi, *Pure Appl. Chem.*, 2003, **75**, 577; (b) S. Fukuzumi, *Electron Transfer in Chemistry*, ed. V. Balzani, Wiley-VCH, Weinheim, Germany, 2001, vol. 4, pp. 3–59; (c) S. Fukuzumi, K. Ohkubo and Y. Morimoto, *Phys. Chem. Chem. Phys.*, 2012, **14**, 8472.

17 (a) J. Park, Y. Morimoto, Y.-M. Lee, W. Nam and S. Fukuzumi, *J. Am. Chem. Soc.*, 2012, **134**, 3903; (b) J. Park, Y.-M. Lee, W. Nam and S. Fukuzumi, *J. Am. Chem. Soc.*, 2013, **135**, 5052.

18 (a) M. S. Taylor and E. N. Jacobson, *Angew. Chem., Int. Ed.*, 2006, **45**, 1520; (b) T. Akiyama, *Chem. Rev.*, 2007, **107**, 5744.

19 J. Yuasa, T. Suenobu and S. Fukuzumi, *ChemPhysChem*, 2006, **7**, 942.

20 (a) T. H. Yosca, R. K. Behan, C. M. Krest, E. L. Onderko, M. C. Langston and M. T. Green, *J. Am. Chem. Soc.*, 2014, **136**, 9124; (b) T. H. Yosca, J. Rittle, C. M. Krest, E. L. Onderko, A. Silakov, J. C. Calixto, R. K. Behan and M. T. Green, *Science*, 2013, **342**, 825.

21 (a) L. R. Widger, C. G. Davies, T. Yang, M. A. Siegler, O. Troeppner, G. N. L. Jameson, I. Ivanović-Burmazović and D. P. Goldberg, *J. Am. Chem. Soc.*, 2014, **136**, 2699; (b)

R. Latifi, M. A. Sainna, E. V. Rybak-Akimova and S. P. de Visser, *Chem. - Eur. J.*, 2013, **19**, 4058.

22 (*a*) R. A. Marcus, *Annu. Rev. Phys. Chem.*, 1964, **15**, 155; (*b*) R. A. Marcus and N. Sutin, *Biochim. Biophys. Acta, Rev. Bioenerg.*, 1985, **811**, 265; (*c*) R. A. Marcus, *Angew. Chem., Int. Ed. Engl.*, 1993, **32**, 1111.

23 J. Chen, Y.-M. Lee, K. M. Davis, X. Wu, M. S. Seo, K.-B. Cho, H. Yoon, Y. J. Park, S. Fukuzumi, Y. N. Pushkar and W. Nam, *J. Am. Chem. Soc.*, 2013, **135**, 6388.

24 H. Yoon, Y.-M. Lee, X. Wu, K.-B. Cho, R. Sarangi, W. Nam and S. Fukuzumi, *J. Am. Chem. Soc.*, 2013, **135**, 9186.

25 (*a*) X. Wu, M. S. Seo, K. M. Davis, Y.-M. Lee, J. Chen, K.-B. Cho, Y. N. Pushkar and W. Nam, *J. Am. Chem. Soc.*, 2011, **133**, 20088; (*b*) H. Yoon, Y. Morimoto, Y.-M. Lee, W. Nam and S. Fukuzumi, *Chem. Commun.*, 2012, **48**, 11187.

26 D. F. Evans and D. A. Jakubovic, *J. Chem. Soc., Dalton Trans.*, 1988, 2927.

27 S. Fukuzumi, *Coord. Chem. Rev.*, 2013, **257**, 1564.

28 Y.-M. Lee, H. Kotani, T. Suenobu, W. Nam and S. Fukuzumi, *J. Am. Chem. Soc.*, 2008, **130**, 434.

29 S. Bang, S. Park, Y.-M. Lee, S. Hong, K.-B. Cho and W. Nam, *Angew. Chem., Int. Ed.*, 2014, **53**, 7843.

30 S. Fukuzumi, S. Itoh, T. Komori, T. Suenobu, A. Ishida, M. Fujitsuka and O. Ito, *J. Am. Chem. Soc.*, 2000, **122**, 8435.

31 K.-B. Cho, X. Wu, Y.-M. Lee, Y. H. Kwon, S. Shaik and W. Nam, *J. Am. Chem. Soc.*, 2012, **134**, 20222.